



## Solving the linear radiation problem using a volume method on an overset grid

**Read, Robert; Bingham, Harry B.**

*Published in:*  
International Workshop on Water Waves and Floating Bodies

*Publication date:*  
2012

*Document Version*  
Publisher's PDF, also known as Version of record

[Link back to DTU Orbit](#)

*Citation (APA):*  
Read, R., & Bingham, H. B. (2012). Solving the linear radiation problem using a volume method on an overset grid. In International Workshop on Water Waves and Floating Bodies

---

### General rights

Copyright and moral rights for the publications made accessible in the public portal are retained by the authors and/or other copyright owners and it is a condition of accessing publications that users recognise and abide by the legal requirements associated with these rights.

- Users may download and print one copy of any publication from the public portal for the purpose of private study or research.
- You may not further distribute the material or use it for any profit-making activity or commercial gain
- You may freely distribute the URL identifying the publication in the public portal

If you believe that this document breaches copyright please contact us providing details, and we will remove access to the work immediately and investigate your claim.

# Solving the linear radiation problem using a volume method on an overset grid

Robert Read, Harry Bingham

Department of Mechanical Engineering, Technical University of Denmark,  
2800 Kgs. Lyngby, Denmark.

E-mail: rrea@mek.dtu.dk, hbb@mek.dtu.dk

## Background

This paper describes recent progress towards the development of a computational tool, based on potential flow theory, that can accurately and efficiently simulate wave-induced loadings on marine structures. Engsig-Karup et al. (2009) have successfully developed an arbitrary-order, finite-difference-based, potential-flow model to represent the propagation of fully non-linear waves in coastal regions of varying bathymetry. The present objective is to develop this methodology to include the presence of a floating structure. To represent the curvilinear boundaries of the structure and the bottom, the single-block methodology developed previously is applied to multiple, overlapping grid blocks using the overset approach. While the ultimate aim of this work is to model fully non-linear wave-structure interaction, a linear solver has been initially implemented to permit the use of a fixed grid, and to allow comparison of numerical results with established analytical solutions.

The linear radiation problem is considered in this paper. A two-dimensional computational tool has been developed to calculate the force applied to a floating body of arbitrary form in response to a prescribed displacement. Fourier transforms of the time-dependent displacement and force are applied, and the ratio of the resulting signals used to determine the radiation added mass and damping of the body as a function of frequency. The present software implementation has been validated by comparing numerical results from the linear model with analytical solutions for several test cases. The dynamic behaviour of a cylinder and barge on variable bathymetry has been investigated on a multi-block grid in two dimensions. Simulations have been performed to evaluate the induced flow field and radiation forces generated by these bodies in response to a Gaussian displacement. The hydrodynamic coefficients associated with body motions in surge, heave, and pitch have been calculated and compared with exact solutions. A three-dimensional implementation of the linear model has recently been completed.

## Problem formulation

A Cartesian coordinate system is adopted with the  $xy$ -plane coincident with the undisturbed free surface and the  $z$ -axis directed upwards. The depth of the undisturbed fluid is defined as  $h(\mathbf{x})$ , where  $\mathbf{x} = (x, y)$  is the coordinate vector in the horizontal plane. The free-surface elevation is defined as  $z = \eta(\mathbf{x}, t)$ . Assuming that the fluid is incompressible and inviscid and the flow is irrotational, the fluid velocity  $\mathbf{u} = (u, v, w) = (\nabla\phi, \partial_z\phi)$ , can be expressed as the gradient of a scalar velocity potential  $\phi(\mathbf{x}, z, t)$ , where  $\nabla = (\partial_x, \partial_y)$ . In the linear case, where it is assumed that the wave elevation is small compared to the wavelength, the development of the free surface with respect to time is governed by a kinematic and a dynamic boundary condition as follows

$$\partial_t\eta = \tilde{w}, \quad (1)$$

$$\partial_t\tilde{\phi} = -g\eta, \quad (2)$$

where  $\tilde{w} = w(\mathbf{x}, 0, t)$  and  $\tilde{\phi} = \phi(\mathbf{x}, 0, t)$ . With a knowledge of  $\eta$  and  $\tilde{\phi}$ , these equations are evolved in time by solving Laplace's equation in the fluid domain subject to the condition that the normal component of the fluid velocity at all solid boundaries must be equal to the normal velocity of the boundary itself. Hence,

$$\phi = \tilde{\phi}, \quad z = 0, \quad (3)$$

$$\nabla^2\phi + \partial_{zz}\phi = 0, \quad -h \leq z \leq 0, \quad (4)$$

$$(\mathbf{n}, n_z) \cdot \mathbf{u} = (\mathbf{n}, n_z) \cdot \mathbf{u}_b, \quad (\mathbf{x}, z) \in \partial\Omega, \quad (5)$$

where  $(\mathbf{n}, n_z)$  is a vector directed out of the fluid, normal to the solid boundary surface  $\partial\Omega$ , and  $\mathbf{u}_b$  is the velocity of the boundary. The Neumann boundary condition expressed in Equation 5 is homogeneous for all stationary surfaces and non-homogeneous for moving boundaries. Having identified the velocity potential, the pressure,  $p$ , can be evaluated at every point in the fluid according to the linearised Bernoulli equation,

$$p = -\rho\phi_t \quad -h \leq z \leq \eta. \quad (6)$$

The dynamic forces and moments applied by the fluid to the body can then be calculated by integrating the pressure over the body surface as follows

$$\begin{pmatrix} \mathbf{F} \\ \mathbf{M} \end{pmatrix} = \iint_{S_b} p \begin{pmatrix} \mathbf{n} \\ \mathbf{r} \times \mathbf{n} \end{pmatrix} dS. \quad (7)$$

The frequency-dependent added mass and damping corresponding to each of these degrees of freedom can then be evaluated as the ratio of the Fourier-transformed force and displacement signals as follows

$$a_{ij}(\omega) = \text{Re} \left[ \frac{f\{F_j(t)\}}{f\{\xi_i(t)\}} \right], \quad i, j = 1, 2, 3, \quad (8)$$

$$b_{ij}(\omega) = -\text{Im} \left[ \frac{f\{F_j(t)\}}{f\{\xi_i(t)\}} \right], \quad i, j = 1, 2, 3, \quad (9)$$

where  $f\{\}$  represents the Fourier transform. These values are typically presented non-dimensionalised.

## Numerical solution

The governing equations presented above have been solved numerically using the Overture C++ framework developed by Brown and Henshaw (1998) to solve partial differential equations on multiple, overlapping grid blocks. This framework includes a powerful grid generator, an interface to a variety of sparse elliptic solvers, and parallel processing capabilities. A two-dimensional numerical solution was obtained with fourth-order accuracy in space and time. Centred, finite-difference schemes were developed on a computational grid and weighted to satisfy the governing equations on the physical grid. Laplace's equation was enforced at all internal and boundary points with the exception of the free surface, where a Dirichlet boundary condition was applied. Ghost points were introduced around each block to enforce Neumann boundary conditions at solid surfaces, or to interpolate between grid blocks. A non-homogeneous Neumann boundary condition at the body surface represented displacement. The resulting system of linear equations was solved using the Yale sparse matrix package (Eisenstat et al., 1982). The free-surface elevation and potential at each time step were obtained by a classical Runge-Kutta solution of the free-surface equations. Here, a fixed time-step was used with a Courant number of 0.5. The pressure was evaluated to fourth-order accuracy, and thereafter integrated over the body surface using the left-null-vector method for integration on overlapping grids. Discrete fast Fourier transforms of the generated force and displacement time-series were then performed, and the added mass and damping calculated.

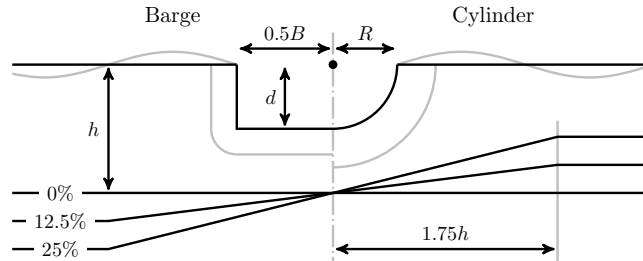


Figure 1: Spatial configuration of shallow test cases. Grey lines offset from the body surfaces represent interpolation boundaries. The line of symmetry applies to the bodies, but not to the bottom surfaces.

## Two-dimensional test cases

Correct implementation of the two-dimensional linear model has been confirmed using two simple test cases: a half-submerged cylinder and a rectangular barge. Time-domain simulations have been conducted in shallow and deep water with flat and inclined bottoms. The radiation added mass and damping have been evaluated for each combination of excitation and response, and the results compared to analytical solutions. The spatial configuration of the shallow grids close to the cylinder and barge is shown in Fig. 1. The cylinder has a non-dimensional radius  $R/h = 0.5$ . The barge has a full non-dimensional width  $B/h = 1.5$  and a draft  $d/h = 0.5$ . The pitch axis in both excitation and response is identified by the filled dot. The lateral distance to the vertical boundaries at either end of the fluid domain (not shown) was sufficiently large to ensure that reflected waves could not significantly influence the body force.

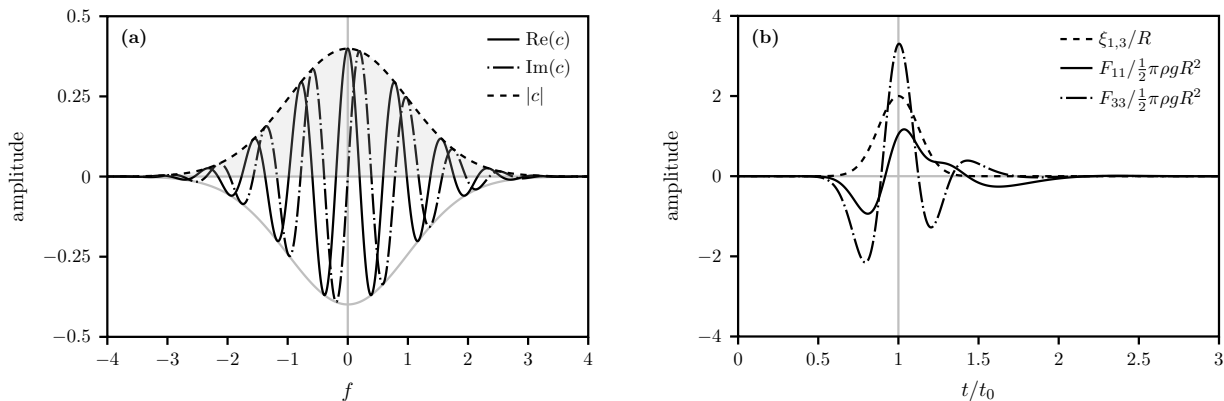


Figure 2: The method of excitation: (a) frequency domain, (b) time domain.

During each simulation, the body displacement was compelled to follow a Gaussian profile, and thereby introduced a Gaussian range of frequencies into the fluid domain. The width of the frequency Gaussian was selected so that the amplitude at the Nyquist frequency was 0.01% of the maximum value at  $f = 0$ . The excitation profiles in the time and frequency domains are shown in Fig. 2, together with the normalized force response calculated for surge and heave of the cylinder over a flat bottom.

## Results

Convergence of the solutions with grid refinement was confirmed. Figs. 3(a) and (b) show the numerical results for cylinder motion over shallow water with a flat bottom, together with the infinite-depth analytical solution calculated using a multipole method (Ursell, 1949). The added mass and damping have been non-dimensionalised as follows:

$$\mu_{ij} = \frac{a_{ij}}{\frac{1}{2}\pi\rho R^2}, \quad \nu_{ij} = \frac{b_{ij}}{\frac{1}{2}\pi\rho\omega R^2}, \quad i, j = 1, 3. \quad (10)$$

Good agreement might reasonably be expected for values of  $kR$  corresponding to  $kh_s > \pi$ , where the waves are sufficiently short to remain unaffected by the bottom. For the shallow-water configuration illustrated in Fig. 1, this agreement is evident in the surge-surge mode. However, the high-frequency asymptotic value of the added mass derived from the heave-heave simulation is significantly higher than the infinite-depth exact solution. This phenomenon results from the shallow depth used in the simulation. The results derived from a deep-water simulation, where  $h/R$  was increased to 3, are included in Fig. 1, and show good agreement to the right of the  $kh_d = \pi$  line, suggesting that the numerical model is correctly evaluating the cylinder's added mass and damping.

The numerical results for barge motion over shallow water with a flat bottom are shown in Figs. 3(c) and (d), together with the analytical solution generated by Liu (2010) using a step method. Here, the

normalization used for the added mass and damping coefficients is given by

$$\tilde{a}_{ij} = \frac{a_{ij}}{\rho h^2}, \quad \tilde{b}_{ij} = \frac{b_{ij} \sqrt{h/g}}{\rho h^2}, \quad i, j = 1, 3. \quad (11)$$

The agreement between the analytical and numerical results is good for the surge-surge and heave-heave modes. Separate results including bottom slope effects show similar agreement, though as for the cylinder test case, the effect of slope on the coefficients is limited. For simulations where the response is evaluated in a mode other than the excitation mode, the responses are smaller and more significant differences between the numerical and exact results are evident. The reasons for these discrepancies are the subject of present investigation. In addition, a three-dimensional implementation of the code is presently being validated using a hemispherical body.

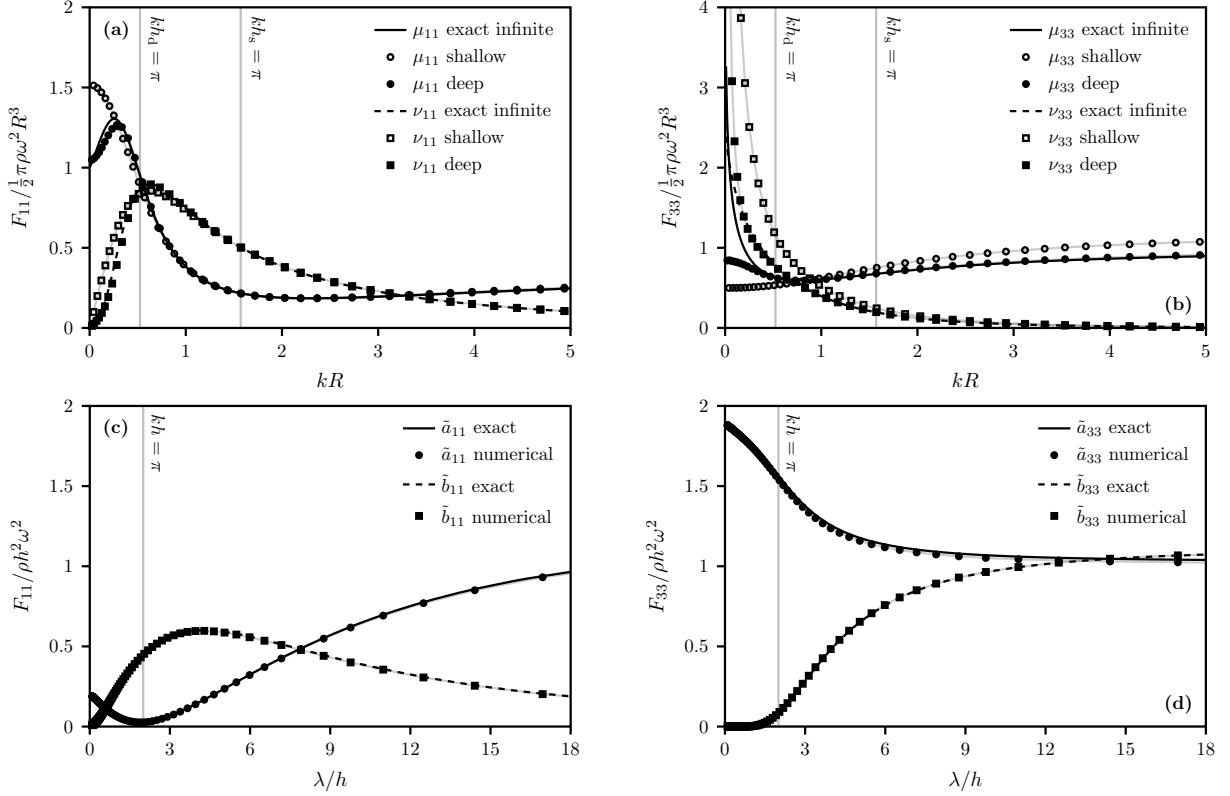


Figure 3: Comparison of numerical and analytical solutions over a flat bottom: (a) cylinder surge-surge, (b) cylinder heave-heave, (c) barge surge-surge, (d) barge heave-heave.

## Acknowledgements

The authors wish to thank the Danish Agency for Science, Technology and Innovation (grant 09-067257) for funding, and the Danish Center for Scientific Computing. We are also grateful to Bill Henshaw for his guidance using Overture, and Richard Porter for suggestions regarding calculation of the multipole solution.

- D. L. Brown and W. D. Henshaw. Overture: Object-oriented tools for solving CFD and combustion problems. In A. Tentner, editor, *Proceedings of the International Symposium on High Performance Computing*, pages 21–26. The Society for Modeling and Simulation International, 1998.
- S. C. Eisenstat, M. C. Gursky, M. H. Schultz, and A. H. Sherman. Yale sparse-matrix package 1: The symmetric codes. *International Journal for Numerical Methods in Engineering*, 18(8):1145–1151, 1982.
- A. P. Engsig-Karup, H. B. Bingham, and O. Lindberg. An efficient flexible-order model for 3D nonlinear water waves. *Journal of Computational Physics*, 228:2100–2118, 2009.
- Y. Liu. *Effects of variable bathymetry on the linear and slow-drift wave responses of floating bodies*. PhD thesis, Université de Provence Aix-Marseille 1, 2010.
- F. Ursell. On the heaving motion of a circular cylinder on the surface of a fluid. *Quarterly Journal of Mechanics and Applied Mathematics*, 2(2):218–231, 1949.